Pure & Appl. Chem., Vol. 62, No. 2, pp. 229–234, 1990.
Printed in Great Britain.

Multidimensional EPR imaging of nitroxides

Minoru Sueki, Gareth R. Eaton, Sandra S. Eaton

Departments of Engineering and Chemistry, University of Denver, Denver, Colorado 80208 USA and Department of Chemistry, University of Colorado-Denver, 1200 Larimer St., Denver, Colorado 80204 USA

Abstract - The information obtained by EPR about a heterogeneous sample depends strongly on the EPR technique used. Even within the class of measurements called EPR imaging very different perspectives are provided by CW and spin-echo detected 2D spectral-spatial images and 3D spectral-spatial-spatial images.

INTRODUCTION

The extensive applications of nitroxide radicals in chemistry, materials sciences, and bio-medical sciences, include many cases in which the distribution of radicals could be non-uniform, and in which this non-uniformity contains important information about the physical system. Consequently, there is strong incentive to perform EPR imaging experiments using nitroxide radicals (ref. 1).

Two important characteristics of EPR imaging are the need to handle a) multi-line spectra such as the spectra of nitroxides and b) spectra with varying linewidths, such as arise for nitroxides with differing mobilities or in the presence of varying amounts of oxygen. Since both hyperfine splitting and linewidths convey potentially important information about the sample, it is desirable to find ways to include these "complexities" in the EPR image rather than just find ways to remove the complications (ref. 2). The approach that we are taking to handle both of these cases is spectral-spatial EPR imaging (ref. 3).

Spectral-spatial EPR imaging gives the full EPR spectrum as a function of position in the sample (ref. 3). Spectra are obtained at a series of magnetic field gradients that correspond to projections in a spectral-spatial plane. The dimensions of the pseudo-object are ΔH in the spectral dimension and L in the spatial dimension. The resolution of the image is a function of the number of experimental projections, the maximum gradient, and the spectral width, ΔH. The resolution can be improved by collecting an incomplete set of experimental projections and doing the image reconstruction with a "missing angle" algorithm. Large spectral widths, ΔH, contribute to decreased spatial resolution of the image. The spectral window might not include the complete spectrum when paramagnetic metals with multi-line spectra and nitroxyls are both present in a sample or when one wants to image only one line of a nitroxyl radical spectrum. The images shown in the Figures were obtained with incomplete data sets and were reconstructed with an iterative algorithm described in ref. 3.

It is also important to recognize that the "image" that one obtains for a particular sample depends strongly in the way one looks at the sample. One gets a different image of the sample when different dimensions are imaged - one spatial dimension vs. two spatial dimensions is obvious. Less obvious, but equally important, are the differences one gets when a variation is made in a dimension such as the time, τ, between pulses in a spin-echo image. In this paper we exhibit several views of one sample to illustrate the variety of appearances of "the EPR image."

RESULTS AND DISCUSSION

For the purpose of this demonstration we constructed a sample that contained two nitroxyl radical specimens, two coal specimens, a specimen of solid DPPH (diphenylpicrylhydrazyl), a fragment of irradiated quartz, and a specimen of

galvinoxyl radical. The galvinoxyl was about 1 mM in degassed toluene solution, and was contained in a 3 mm OD pyrex tube (ca. 1.8 mm ID). One nitroxyl specimen was ^{15}N-tempone (4-oxo-2,2,6,6-tetramethylpiperidin-1-yl-oxy) ca. 2 mM in degassed toluene and sealed in a 0.4 mm pathlength microslide. The other nitroxyl specimen was of the same radical ca. 2 mM in degassed di-orthoxylylethane, sealed in a 4 mm OD pyrex tube (ca. 2.4 mm ID). These specimens were arranged in and around a 5 mm OD NMR tube for support, as sketched in Fig. 1.

The "normal" CW EPR spectrum of this sample is shown in Fig. 2. Under these conditions the irradiated quartz signal is partly saturated, and its relaxation time is too long to obtain a slow-passage EPR spectrum with 100 kHz modulation. A different spectrum would be obtained (not shown) at higher or lower microwave powers and at other modulation frequencies. Hence, even this conventional "normal" EPR spectrum yields information that is strongly dependent on the details of acquisition parameters. One can see the two-line nitroxyl signal and the multi-line galvinoxyl signal superimposed on a broad resonance.

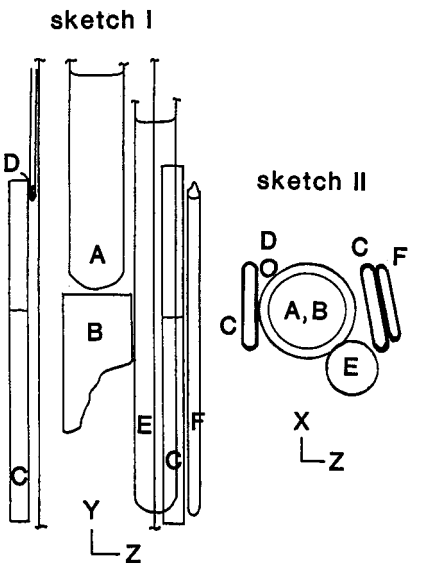

Fig. 1 Sketches of the special sample used in these studies. A is ^{15}N-tempone in di-orthoxylylethane, B is irradiated quartz, C is coal, D is DPPH, E is galvinoxyl, and F is ^{15}N-tempone in toluene. Sketch I is the profile of the sample in the yz plane. Sketch II is the profile in the XZ plane. The Z axis is along the main magnetic field, the Y axis is along the axis of a typical sample tube in the cavity.

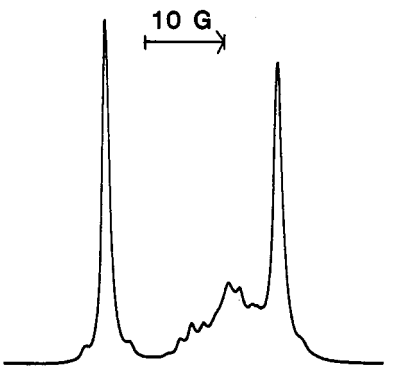

Fig. 2. "Normal" X-band (ca. 9.4 GHz) CW EPR spectrum of the sample shown in Figure 1. The spectrum was obtained with 0.1 gauss 100 kHz magnetic field modulation. It is shown here in integrated form for comparison with the spectral dimensions in other figures.

Using multiple magnetic field gradients (ref. 4) (maximum = 200 G/cm) and reconstructing the image as previously reported (ref. 3), one obtains vastly more information about the sample. For example, it is clearly seen in Fig. 3 that the sample is heterogeneous, consisting (at least) of regions of coal, then DPPH, then nitroxyl, then galvinoxyl, then coal, then nitroxyl again. Refering to the composition of the sample (Fig. 1) it is seen that some features of the sample are not yet revealed. Fig. 4 is similar to Fig. 3, but with lower maximum Z-gradient (100 G/cm), and hence poorer spatial resolution. It is included for comparison with the succeeding Figures, which were all obtained with the smaller Z-gradient strength.

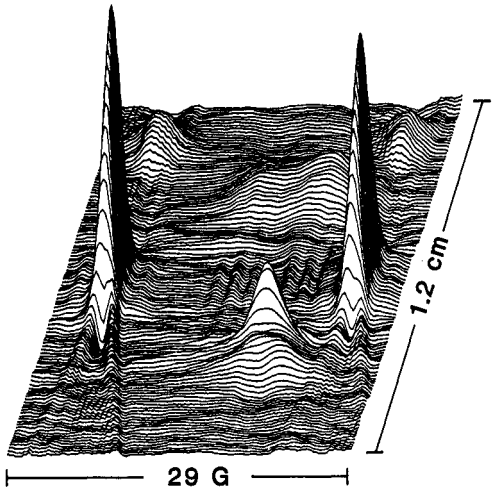

Fig. 3. Spectral-spatial X-band CW EPR image of the sample shown in Fig. 1. The image was obtained with a maximum Z-gradient of 200 G/cm. The Y-axis positioning of the sample for this image was about 2 mm different than that for the other images in this paper, which resulted in an increased intensity for the nitroxyl sample in tube A.

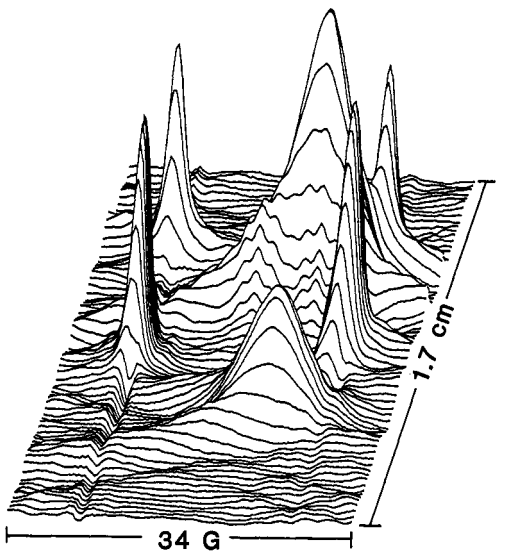

Fig. 4. Spectral-spatial X-band CW EPR image of the sample shown in Fig. 1. The image was obtained with a maximum Z-gradient of 100 G/cm.

A full 3D YZ-spectral data set (ref. 5) for this sample involves 900 EPR spectra, each with a different combination of Y and Z gradients. These constitute 30 experimental and two "missing" projections in each of 30 spatial planes. Upon reconstruction, the YZ spin density map in Fig. 5 is obtained. As we have previously shown, when obtained in this way, the data can be displayed to reveal, for example, the full field-swept hyperfine-split EPR spectrum at any point in the 2D spatial-spatial (YZ) plane. One of these spectra is presented in Fig. 8a. One could also present the spatial-spatial (YZ) distribution of spin density at any chosen magnetic field strength. For example, if the magnetic field corresponding to the low-field line of the nitroxyl radical were selected, the YZ contour plot would show that the upper region of the spin density map was due almost entirely to nitroxyl radicals, and the right-hand part of the right-hand region of the spin density plot is due to nitroxyl radicals (Fig. 9a). The sample with the nitroxyl spin density in the upper region of the spin density map actually was a long cylinder extending above the top of the cavity. However, the Y dimension of the cavity is less than the Y dimension of the image, so the image is truncated at the top of the cavity. Furthermore, the image is not corrected for the distribution of microwave B_1 and magnetic field modulation in the cavity. Hence, the amplitude of the signals in the image away from the center of the cavity is attenuated in the Y direction of the image.

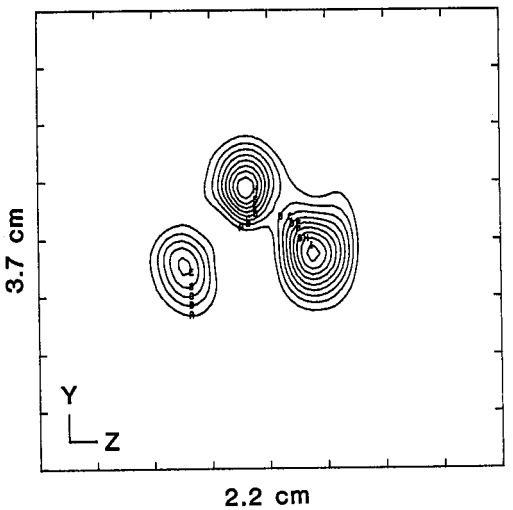

Fig. 5. Spectral-spatial-spatial 3D X-band CW EPR image of the sample shown in Fig. 1. The image was obtained with a maximum Y-gradient of 60 G/cm and a maximum Z-gradient of 100 G/cm.

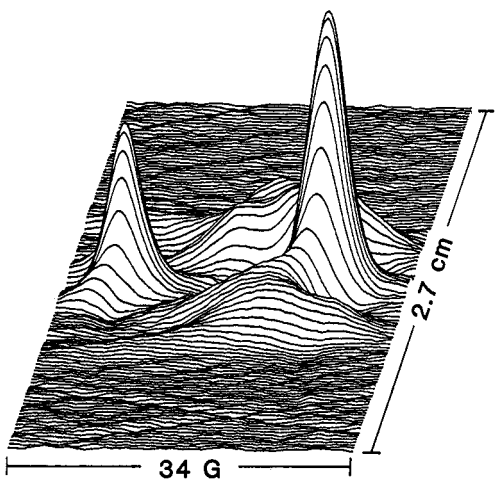

Fig. 6. Spectral-spatial field-swept X-band spin echo-detected EPR image of the sample shown in Fig. 1. The image was obtained with a maximum Z-gradient of 100 G/cm. The time between the two pulses was 250 ns.

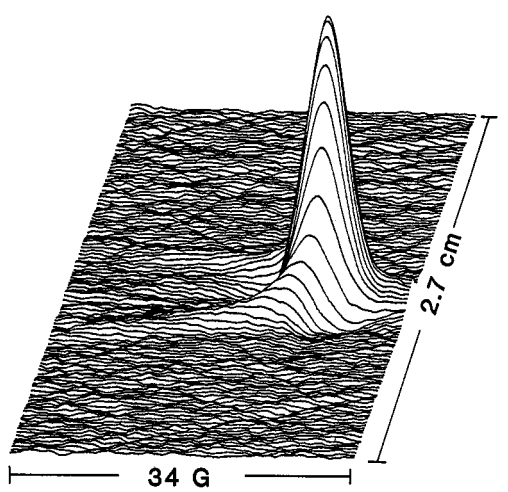

Fig. 7. Spectral-spatial field-swept X-band spin echo-detected EPR image of the sample shown in Fig. 1. The image was obtained with a maximum Z-gradient of 100 G/cm. The time between the two pulses was 1000 ns.

Another relevant dimension to consider is the relaxation time of the radicals (ref. 6). Images constructed from spin-echo-detected EPR spectra (ref. 7) can be much more revealing, and as we shall see, much less revealing, of the details of the sample. The echoes observable for the same sample when the time between microwave pulses is 250 nsec yield the Z-spectral image presented in Fig. 6. The echo-detected image is dominated by the irradiated quartz signal, which was negligible in the CW image. The nature of this detection technique yields spectra that are broader than the usual CW field-swept spectra. Nevertheless, the coal, nitroxyl, coal sequence in the sample is evident. Conspicuously missing is the second (right-hand in Fig. 1) nitroxyl sample. This nitroxyl sample does not show up in this image because the T_2 of the nitroxyl in toluene solution is so much shorter than that of the nitroxyl in the more viscous di-orthoxylylethane, that its echo has decayed to the noise level by 250 nsec after the pulse. When the echoes are detected 1 microsec after the pulse, only the irradiated quartz signal is still above the noise level. An image constructed at this time (Fig. 7) shows this complex sample to consist simply of one particle of quartz - everything else has been missed! This effect could be turned to advantage - to image only the slowly relaxing spins in a sample.

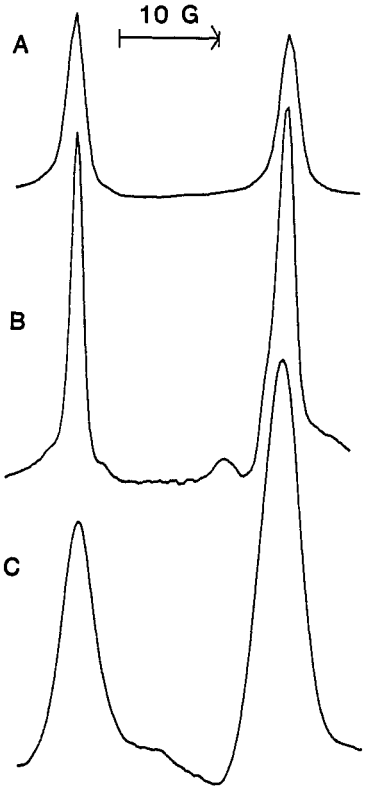

Fig. 8. Comparison of EPR spectra extracted from the images shown in previous Figures. In each case the spectra are presented as absorption spectra, with the horizontal axis the magnetic field scan. The spacing between the nitroxyl lines is ca. 22 G, and serves to define the magnetic field scale. (a) EPR spectrum from the YZ coordinate in Fig. 5 corresponding to the location of the ^{15}N-tempone in di-ortho-xylylethane. (b) EPR spectrum from the Z coordinate in Fig. 4. corresponding to the location of the ^{15}N-tempone in di-ortho-xylylethane. A small peak due to DPPH occurs between the two nitroxyl lines. (c) EPR spectrum from the Z coordinate in Fig. 6. corresponding to the location of the ^{15}N-tempone in di-ortho-xylylethane. The quartz peak is superimposed on the high-field nitroxyl line.

The spatial distribution of nitroxyl radicals in this sample is revealed differently (Fig. 9) by the three fundamentally different perspectives of the sample presented here. The spin-echo image (Fig. 6) detected only the nitroxyl (Fig. 9c) in the more viscous solvent. The CW image (Fig. 4) detected both nitroxyl specimens and their separation along the Z-axis Fig. 9b). The 3D CW YZ-spectral image (Fig. 5 and 8a) shows the location of both nitroxyl samples in the YZ plane (Fig. 9a).

Acknowledgement

This work was supported in part by NSF grant CHE-8722804.

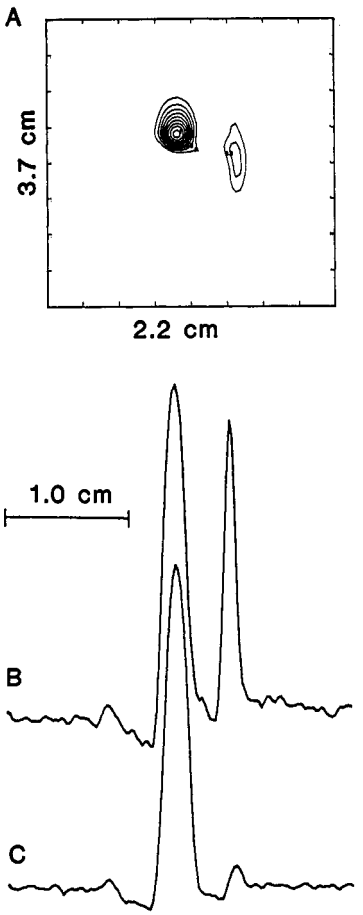

Fig. 9. Spatial distribution of nitroxyl radicals revealed by the imaging experiments in the previous Figures. These are plots of intensity as a function of distance at the magnetic field position corresponding to the low-field EPR line of the nitroxyl radical. (a) from the 3D spectral-spatial-spatial image of Fig. 5. The vertical orientation of the nitroxyl specimen in the thin microslide is evident. (b) from the CW 2D spectral-spatial image of Fig. 4; and (c) from the ESE-detected 2D spectral-spatial image of Fig. 6. The nitroxyl spectrum in toluene shows up in the CW images, but not in the ESE images.

REFERENCES

1. G. R. Eaton and S. S. Eaton, Bull. Magn. Reson. 10, 22 (1988).

2. G. R. Eaton and S. S. Eaton, in Electron Magnetic Resonance of the Solid State, J. A. Weil, M. K. Bowman, J. R. Morton, and K. F. Preston, eds., The Canadian Society for Chemistry, 1987, p. 639

3. M. M. Maltempo, S. S. Eaton, and G. R. Eaton, J. Magn. Reson. 77, 75 (1988).

4. S. S. Eaton and G. R. Eaton, Spectroscopy 1, 32 (1986).

5. S. S. Eaton, M. M. Maltempo, E. D. A. Stemp, and G. R. Eaton, Chem. Phys. Lett. 142, 567 (1987).

6. G. R. Eaton and S. S. Eaton, J. Magn. Reson. 67, 73 (1986).

7. R. W. Quine, G. R. Eaton, and S. S. Eaton, Rev. Sci. Instrum. 58, 1709 (1987).